Stability of liquid sheet edges

R. Krechetnikov
Department of Mechanical Engineering, University of California, Santa Barbara, California 93106, USA

(Received 22 December 2009; accepted 12 July 2010; published online 7 September 2010)

Accelerating edges of thin liquid sheets are ubiquitous and are known to experience a longitudinal (along-the-edge) instability, which often leads to their break-up and atomization. The fundamental physical mechanisms of this instability are studied analytically in the quasisteady regime, which admits a concise modeling. It is discovered that the classical Rayleigh–Taylor mechanism is substantially modified which leads to a stability picture different from that for flat interfaces, in part due to an interplay with Rayleigh–Plateau mechanisms. In particular, as the Bond number increases, first, only one critical wavenumber is excited, but for higher values of the Bond number several critical wavenumbers can coexist with the same growth rates. This allows for the transition from the regular picture, in which one wavelength sets the pattern, to the frustrated picture, in which a few wavenumbers compete with each other. © *2010 American Institute of Physics*.
[doi:10.1063/1.3474640]

I. INTRODUCTION

A. The phenomena of liquid sheet edges

Liquid sheets are ubiquitous, from waterfalls and splashes to numerous applications such as curtain coating[1,2] and atomization.[3] Regardless of the physical situation, liquid sheets are bounded and thus have edges, which have always been of interest, e.g., in the context of liquid curtains,[1,2,4] since they are the gateways to liquid sheet disintegration and atomization. Liquid edges may be present in an apparently steady form, such as in the case of an impact of a continuous water jet on a disk,[5,6] or in a highly unsteady fashion, as in the case of a water drop impact on a small target disk.[7] The sources of unsteadiness of liquid edges are the external forces (e.g., gravity or inertial effects as in the drop impact problems[7–9]) and the retraction phenomena due to surface tension.

The retraction effects have been studied in the inviscid approximation using a macroscopic momentum balance by Taylor[10] and by Culick,[11] who calculated the retraction velocity, and later by Keller,[12] who extended the previous analyses to liquid sheets of nonuniform thickness. The case of viscous retraction was analyzed by Brenner and Gueyffier[13] using the lubrication approximation, which allowed them, in particular, to explain the existence of flat retracting edges observed earlier in experiments in Refs. 14 and 15 and caused by the domination of viscous effects over the capillary ones. The same problem of retraction was studied numerically as well, cf. Refs. 16 and 17.

Despite extensive studies of the retraction processes, the longitudinal (called here "along-the-edge") instability, sketched in Fig. 1, has not received much systematic attention. The only two theoretical works on the subject—by Roisman *et al.*[18] and by Fullana and Zaleski[19]—are based on phenomenological treatments, which nevertheless required numerical solution of phenomenologically formulated equations, and produced contradictory results. Namely, in the limit when the edge develops into a blob attached to a thin liquid sheet, the problem was studied phenomenologically by Fullana and Zaleski,[19] who followed the Rayleigh–Plateau analysis for jet break-up and concluded that the growing retracting edge does not typically break into droplets for moderate wavelengths. Besides retraction, other unsteady effects, such as acceleration and a time-dependent sheet thickness, were not taken into account in that work. On the other hand, the work by Roisman *et al.*,[18] based on the phenomenological momentum balance, predicted instability, which they attributed solely to the Rayleigh–Plateau mechanism, thus contradicting the conclusion of the work of Fullana and Zaleski.[19] Above, we reviewed only the facts, which are relevant to our present discussion, while the reader can learn more about liquid sheets from the book by Lin[20] and review articles by Sirignano and Mehring[21] and Clanet.[5]

In conclusion, one has to admit that there are no rigorous predictive models for the evolution of liquid sheet edges, which is due to the lack of understanding of the underlying fundamental mechanisms. While instability of accelerated *flat* interfaces of infinite extent (the Rayleigh–Taylor instability) is well-studied, it is known that it is not applicable to curved interfaces, as shown in Ref. 22 in the case of slightly perturbed flat base state interfaces. There have been attempts to apply the classical Rayleigh–Taylor analysis developed for flat interfaces to liquid sheet edges, e.g., in the context of the drop splash problem by Allen,[23] but, as expected, without much success in explaining the number of spikes in the drop splash crown.[8,9,24–26] On the other hand, static interfaces with positive curvature (convex interfaces) are known to be subject to the Rayleigh–Plateau instability,[27] so one can expect a simultaneous presence and interplay of both Rayleigh–Taylor and Rayleigh–Plateau mechanisms in the case of accelerating liquid sheet edges. As we will see from the analysis in Sec. II D, the presence of a sufficiently strong acceleration, independent from that due to retraction, simplifies the problem substantially, compared to the one studied by Roisman *et al.*[18] and Fullana and Zaleski,[19] and allows a systematic treatment.

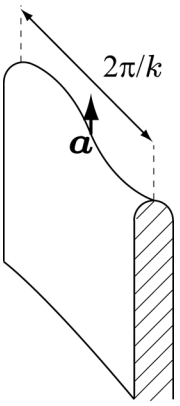

FIG. 1. Along-the-edge instability; k is the wavenumber and $\boldsymbol{a}$ is the acceleration.

Therefore, the focus of this work will be on accelerating liquid sheet edges, whose thickness is comparable to the capillary length, so that surface tension is a leading order effect and thus both Rayleigh–Taylor and Rayleigh–Plateau mechanisms coexist. Only along-the-edge stability of flat liquid sheets will be considered here; such a configuration occurs in a number of physical situations, some of which are sketched in Fig. 2, i.e., a flat liquid sheet cut along a straight line in a gravity field, a splash of a jet on a narrow target, and water hammering. However, the results of the analysis are applicable to other geometries such as rims of large enough radius such that the liquid sheet can be locally considered as flat, as it occurs under certain conditions in the problems of drop splash, curtain coating, and atomization. We will treat three limiting situations: the flattop edges [Fig. 3(a)], rounded edges [Fig. 3(b)], and blob-edges [Fig. 3(c)]. The goal will be to uncover the role and interplay of the surface tension and inertial mechanisms in the origin and evolution of along-the-edge instabilities and to develop their quantitative theory.

B. Paper outline

This paper is organized as follows. First, in Sec. II, we pose the problem and discuss the theoretical prerequisites necessary for the stability study of accelerating liquid sheet edges. With this background, in Sec. III, we then study the stability of ideal flat edges and discover the key new phenomena associated with the along-the-edge instability. Given these basic results in Sec. III B, we then investigate the effects of unsteadiness (namely, due to time-dependence of liquid sheet thickness and retraction) and in Sec. IV, the effects of the curvature of liquid edges; the latter requires a new method of constructing a general solution of the Laplace equation analytically on complex domains, which is offered in this work. The study would be incomplete without a discussion of instability of well-developed blob-edges in Sec. V.

II. THEORETICAL PREREQUISITES

In this section we first provide a general formulation for the stability study of accelerated edges (Sec. II A). For the purpose of further discussion, we then review the classical Rayleigh–Taylor theory in Sec. II B: This is important for understanding why the classical Rayleigh–Taylor theory is not applicable to studying instabilities of liquid sheet edges (Sec. II C). Next, since the accelerating edges of liquid sheets are characterized by two key phenomena—the along-the-edge instabilities and retraction—we then estimate the characteristic time scales of retracting sheets (Sec. II D) based on the classical Taylor–Culick theory, which allows us to define the quasisteady regime to which the subsequent

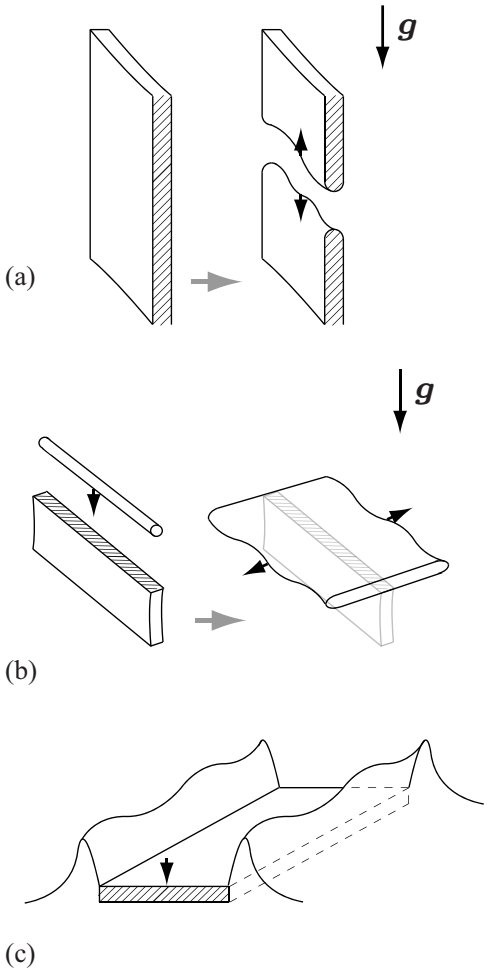

FIG. 2. Accelerating edges of flat liquid sheets due to external body forces (a) and due to inertia [(b) and (c)]. (a) Cut liquid sheet in a gravity field, (b) jet splash on a narrow target, and (c) water hammering.

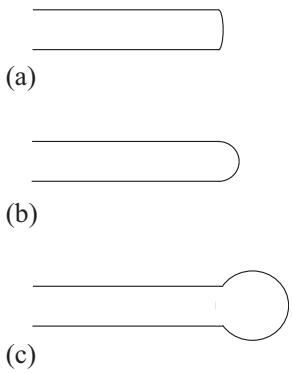

FIG. 3. Three types of edges: (a) flat edge, (b) rounded edge, and (c) blob-edge.

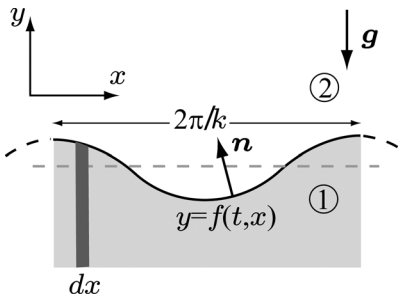

FIG. 4. Two-dimensional interface between two fluids.

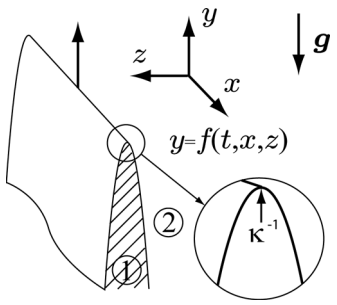

FIG. 5. Interface between two fluids: three-dimensional edge.

analysis applies. While the analysis in this section is done in dimensional variables in order to make various physical effects transparent in Sec. II D, we introduce a nondimensionalization which will be used throughout the remainder of the paper.

A. General problem statement

In the stability analysis of liquid interfaces we consider an inviscid and incompressible approximation of irrotational fluids, i.e., Kelvin's restrictive assumption,[28] usual in the analysis of Rayleigh–Taylor and Rayleigh–Plateau instabilities. Let a general configuration of the interface $y=f(t,x,z)$ [or implicitly $F=y-f(t,x,z)=0$] between two fluids in a body force field $\boldsymbol{g}$, be as in Fig. 4; the body force is either due to gravity or due to transformation to the noninertial coordinate system moving with the accelerating interface (we use the same symbol $\boldsymbol{g}$ for acceleration regardless of the physical origin of the body force). For simplicity of notation, we consider phase 2 inertialess, while the bulk dynamics in phase 1 of incompressible fluid of density ρ is governed by the Laplace equation for the velocity potential ϕ, defined such that $\boldsymbol{u}=\nabla\phi$. In the frame of reference moving with the interface (similar to the analysis of Taylor[10]), this results in the following system for the bulk and interface dynamics:

$$y \le f(t,x,z): \quad \begin{cases} \Delta\phi = 0, \\ |\nabla\phi| < \infty, \quad y \to -\infty, \end{cases} \tag{1a}$$

$$y \le f(t,x,z): \quad \frac{\partial\phi}{\partial t} + \frac{1}{2}|\nabla\phi|^2 = -\frac{1}{\rho}p - gy + C(t), \tag{1b}$$

$$y = f(t,x,z): \quad p = -\sigma\nabla\cdot\boldsymbol{n}, \tag{1c}$$

$$y = f(t,x,z): \quad \frac{\partial F}{\partial t} + \nabla\phi\cdot\nabla F = 0, \tag{1d}$$

where $\boldsymbol{n}$ is the outer normal vector, $\Delta=\partial_x^2+\partial_y^2+\partial_z^2$ is the Laplacian, and $C(t)$ is a time-dependent constant in the Lagrange–Cauchy integral (1b), which is the unsteady version of the Bernoulli integral for potential flow.[29]

As one can learn from Eq. (1), a liquid sheet with an edge cannot exist in a steady state with the interface $f_0(x,z)$ unless such an external pressure distribution P_0 is applied along the interface, which supports the interface shape as in Fig. 5, $P_0/\rho=-gf_0+\sigma\nabla\cdot\boldsymbol{n}/\rho$. In particular, if the pressure of the surrounding phase $P_0=0$, then surface tension force will cause the interface to retract according to the Taylor–Culick theory.[10,11]

B. Classical Rayleigh–Taylor theory for flat interfaces

As a first step towards understanding instabilities of accelerating interfaces, let us consider, for simplicity, a two-dimensional perturbation of a *flat* interface between two phases, one of which is inertialess, as in Fig. 4. The standard way to analyze this problem is to linearize Eq. (1) around the flat interface base state, $f_0=0$, i.e., $f(t,x)=f_0+f'(t,x)=f'(t,x)$ and similarly for $p(t,x,y)$ and $\phi(t,x,y)$,

$$\frac{\partial\phi'}{\partial t} = -\frac{1}{\rho}p' - gf', \quad y \le 0, \tag{2a}$$

$$p' = -\sigma f'_{xx}, \quad y = 0, \tag{2b}$$

$$\frac{\partial f'}{\partial t} = \frac{\partial\phi'}{\partial y}, \quad y = 0, \tag{2c}$$

where the velocity potential ϕ' satisfies the elliptic problem

$$\Delta\phi' = 0, \tag{3a}$$

$$|\nabla\phi'| \to 0, \quad y \to -\infty. \tag{3b}$$

Representing both the velocity potential and the interface perturbation in terms of the Fourier harmonics,

$$\phi'(t,x,y) = \int A_k(t)e^{ikx+|k|y}\mathrm{d}k, \tag{4a}$$

$$f'(t,x) = \int f_k(t)e^{ikx}\mathrm{d}k, \tag{4b}$$

where Eq. (4a) is the formal solution of the Laplace equation (3), and substituting them into Eq. (2) gives the second order oscillator equation

$$\frac{\mathrm{d}^2 f_k}{\mathrm{d}t^2} + \alpha f_k = 0, \quad \alpha = |k|\left[\frac{\sigma}{\rho}k^2 + g\right]. \tag{5}$$

Note that Eq. (5) stays the same in the three-dimensional case with the only difference that the scalar wavenumber k should be replaced with the two-dimensional wavenumber $k\to\boldsymbol{k}=(k_x,k_y)$. For the purpose of further development, it is important to note that in order to solve Eq. (2), one needs a

general solution of the Laplace equation (3), not one for some specific boundary condition. The dispersion relation corresponding to Eq. (5) is

$$\lambda^2 = -|k|\left[\frac{\sigma}{\rho}k^2 + g\right], \tag{6}$$

where λ is the growth rate, which indicates that instability is present if $(\sigma/\rho)k^2+g<0$, i.e., $g<0$, and that the maximum growth rate λ_* occurs for the wavenumber defined by the extremum

$$\frac{d\lambda^2}{dk} = 0 \Rightarrow k_*^2 = -\frac{g}{3}\frac{\rho}{\sigma}, \quad \lambda_* = \left[\frac{4}{27}\frac{\rho}{\sigma}(-g)^3\right]^{1/4}. \tag{7}$$

While the above formal analysis is standard,[28] it does not highlight certain physical aspects of the instability relevant to our discussion, such as a trivial one [What is the physical meaning behind $|k|$ in Eq. (5)?] and the key questions as to what would be different if the base state interface is not flat. Thus, in order to get better insight into the physics of Eq. (5), let us look at the Rayleigh–Taylor instability from the first principles in Sec. II C.

C. Why is the classical Rayleigh–Taylor theory not applicable to edges?

First, notice that Eq. (5), upon multiplication by df_k/dt and integration, yields

$$\left(\frac{df_k}{dt}\right)^2 + \alpha f_k^2 = \text{const}, \tag{8}$$

and thus suggests that this conservative problem has a very simple physical structure, namely, its energy is just a sum of kinetic and potential components. In view of the linearity of the problem, Eq. (8) is the energy of the mode having wavenumber k, which is decoupled from other wavenumbers. Thus, one should be able to derive first Eq. (8) and then Eq. (5).

Consider a perturbation of a wavenumber k and the liquid column of thickness dx as dark shaded in Fig. 4. When the interface is deflected from the flat one, $y=0$, this liquid column attains the following changes in potential energies:

$$\Delta\Pi_g = \tfrac{1}{2}g\rho f^2 dx, \tag{9a}$$

$$\Delta\Pi_\sigma = \sigma(\sqrt{1+f_x^2}-1)dx \simeq \sigma f_x^2/2, \tag{9b}$$

due to acceleration and surface tension, respectively. The kinetic energy is less straightforward since the mass of the column, which attains an increment in the kinetic energy, is defined not by the deflection f from the flat interface position, but by the depth of penetration of the perturbation into the bulk. As we know from solution (4a) of the Laplace equation (3), in the flat interface case the depth of penetration is of the order of the wavelength $\sim k^{-1}$ of the perturbation. Therefore, the change in the kinetic energy should be of the form

$$\Delta T \simeq \frac{1}{2}\rho|k|^{-1}\left(\frac{df}{dt}\right)^2 dx. \tag{10}$$

Next, since the system is conservative, the sum of the changes of potential (9) and kinetic (10) energies of the perturbation $f(t,x)=2f_k(t)\cos kx$, integrated over the wavelength $2\pi/k$, should vanish. The fundamental reason why this sum needs to be integrated over the wavelength is that the linear problem is nonlocal in the physical space (and thus the equation for $f(t,x)$ is integrodifferential), while in the wavenumber space the problem becomes local. Again, it is important to stress that the origin of the factor $|k|$ in Eq. (5) is due to the depth of penetration of the perturbation of wavenumber k into the bulk.

Given the above understanding of the flat interface case, let us consider the long-wave perturbation of a three-dimensional edge having the curvature κ, as illustrated in Fig. 5. As one can immediately guess, the key difference from the flat interface case will be the depth of penetration of the k-wavenumber perturbation (which is dictated by the solution of the Laplace equation), as will be demonstrated in Secs. III and IV, and thus, this difference will affect the kinetic energy estimate. This in turn will modify the instability growth rate since the factor $|k|$ in Eq. (5) should be replaced by a general function of the wavenumber k and curvature κ.

In addition, one should expect another important input to the instability due to the geometry of edges being that between flat interfaces and circular jets. Namely, the geometric configuration of an edge may make it susceptible to the Rayleigh–Plateau instability mechanism, although modified from the classically studied free jet case.[28,30]

D. Characteristic time scales and nondimensionalization

In what follows, for convenience, we will work with nondimensional variables, which are introduced (without using new symbols) via

$$(\boldsymbol{x},f) \to L(\boldsymbol{x},f), \quad t \to (L/a)^{1/2}t, \quad \phi \to L^{3/2}a^{1/2}\phi,$$
$$p \to \rho\ Lap, \quad g \to ag, \tag{11}$$

where L is the characteristic length scale of the physical system, e.g., the liquid sheet thickness h, and $a>0$ is a suitable constant acceleration. As a result of this nondimensionalization, the effect of surface tension is expressed in terms of the Bond number

$$\text{Bo} = \frac{\rho L^2 a}{\sigma}, \tag{12}$$

which measures the ratio of inertial to surface tension forces.

As follows from the Taylor–Culick analysis[10,11] of retraction, the characteristic time scale can be estimated as

$$t_{\text{ret}} = h_s/U_c \sim t^*\text{Bo}^{1/2}, \tag{13}$$

where $t^*=(L/a)^{1/2}$ and $U_c=\sqrt{2\sigma/\rho h}$ is the asymptotic retraction speed reached at $t\to+\infty$. On the other hand, the characteristic time of the Rayleigh–Taylor instability (based on the analysis of the flat interface case in Sec. II B) is

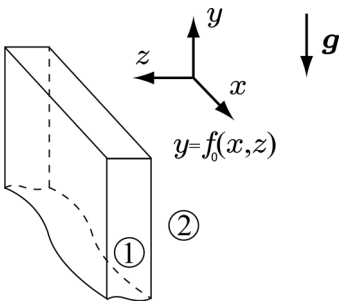

FIG. 6. Base state with flat edge.

$$t_{\text{ins}} = 1/\lambda_* \sim t^* \text{Bo}^{-1/4}, \tag{14}$$

where λ_* is the maximum growth rate defined by Eq. (7). While the above estimate for the characteristic instability time is made using the stability analysis for flat interfaces, the subsequent study will prove that this estimate does not change for liquid sheet edges: an appropriate remark will be made in due course.

Based on formulas (13) and (14), one can introduce a simplification, which will allow us to study the problem analytically and thus to extract the key aspects of the phenomena. Namely, because of the separation of retraction (13) and instability (14) time scales for $\text{Bo} \gg 1$, when instability development is clearly faster than retraction, one can treat the stability problem of unsteady accelerating liquid sheet edge in a quasisteady manner, i.e., one can assume that the base state is "frozen" in time. Such regime is justified, in particular, in the case of large magnitude accelerations as it occurs, for example, in the early stage of the drop impact on a fluid film,[9] when acceleration of the ejected sheet achieves values of at least 10^5 m/s. Similar large accelerations of liquid sheets are observed in the impact of a jet on a solid, cf. Fig. 2(b), and in the water hammering problem, cf. Fig. 2(c).

III. IDEAL FLAT EDGES

By an ideal flat edge base state, we understand the one sketched in Fig. 6. This is a useful idealization, since it allows one to formulate the key phenomena succinctly and serves as a starting point for further analysis in Secs. IV and V (though flat edges with smoothed out corners are observed under certain conditions, e.g., for viscous sheets[13]; here, however, we treat the case of inviscid irrotational fluid motion[31]). The flat edge shown in Fig. 6 is the base state upon which a disturbance field in both x and y directions is imposed. In this work we are concerned with the along-the-edge instability only and therefore disregard any instability on the vertical (with respect to the acceleration $\boldsymbol{g}$) sides based on the following two observations. First, the vertical sides are not accelerating and thus are not subject to the Rayleigh–Taylor instability, i.e., should we include the boundary conditions on the sides, they will not enter the right-hand side of Eq. (16a) as the acceleration is orthogonal to the (x,z)-plane. Second, we are interested in the along-the-edge instability with the largest growth rate and thus the most energetic mode of this instability. The latter clearly can be achieved only if the vertical sides stay unperturbed since nonzero perturbations of the vertical sides would reduce the energy of the along-the-edge perturbation. This is due to the fact that the total energy of all perturbations comes from the hydrostatic (Rayleigh–Taylor) and surface tension (Rayleigh–Plateau) components of the potential energy of the base state of the system, which is conservative. On the basis of the above arguments, the boundary conditions on the vertical sides are considered to be trivial in the subsequent analysis.

A. Constant thickness liquid sheets

Starting from system (1), and taking into account that the normal vector and its gradient are given by

$$\boldsymbol{n} = \frac{-\boldsymbol{i}f_x + \boldsymbol{j} - \boldsymbol{k}f_z}{\sqrt{1+f_x^2+f_z^2}}, \tag{15a}$$

$$\nabla \cdot \boldsymbol{n} = -\frac{f_{xx}(1+f_z^2) - 2f_x f_z f_{xz} + f_{zz}(1+f_x^2)}{(1+f_x^2+f_z^2)^{3/2}}, \tag{15b}$$

respectively, the linearization around the flat edge base state $f_0 = \text{const}$ in the quasistatic approximation gives

$$\frac{\partial \phi'}{\partial t} = -p' - gf', \tag{16a}$$

$$\frac{\partial f'}{\partial t} = -\phi'_y, \tag{16b}$$

$$p' = \text{Bo}^{-1}(f'_{xx} + f'_{zz}), \tag{16c}$$

where the velocity potential is the solution of the Laplace equation (1a). Using separation of variables, one finds that the general solution of Eq. (1a) is given by

$$\phi'(t,x,y,z) = \int_{\mathbb{R}} \sum_{n=-\infty}^{\infty} \phi_{kn}(t) e^{ikx} e^{\sqrt{k^2+n^2}y} e^{inz} \mathrm{d}k, \tag{17}$$

where n is the discrete wavenumber in the z-direction and k is the continuous wavenumber in the x-direction. Solution (17) confirms the intuition developed in Sec. II C that the perturbation penetrates into the bulk at the distance dependent on both the wavenumber k and the sheet thickness, equal to 2π in nondimensional units. In the long wavelength limit, $k \ll 1$, the penetration of perturbation is at the depth of $O(1)$, as suggested by Eq. (17), instead of k^{-1}, as it would be for flat interface. As will be shown next, this also affects the growth rate and the critical wavenumber selection.

Analyzing system (15c) in a manner similar to that in Sec. II B, we find that the linear evolution of the Fourier coefficient f_{kn} of f' obeys

$$\frac{\mathrm{d}^2 f_{kn}}{\mathrm{d}t^2} + \sqrt{n^2+k^2}\{\text{Bo}^{-1}(n^2+k^2) - g\} f_{kn} = 0. \tag{18}$$

The corresponding dispersion relation

$$\lambda^2 = -\sqrt{n^2+k^2}\{\text{Bo}^{-1}(n^2+k^2) + g\}, \tag{19}$$

suggests that the growth rate λ depends only on the modulus of the two-dimensional wavenumber $(k^2+n^2)^{1/2}$ and thus is

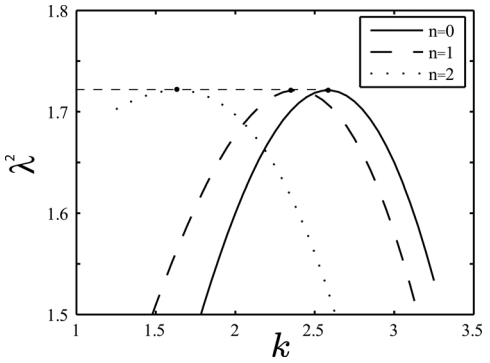

FIG. 7. Growth rates and wavenumber selection: Bo=20 and $g=1$.

structurally the same as Eq. (6). Therefore, the scaling for λ_* does not change and the characteristic time of instability (14) stays intact, which justifies the quasisteady approximation used here. The maximum growth rate $\lambda^*=\max\lambda$ is achieved at

$$\lambda^* = \lambda|_{k^*=\sqrt{-(g/3)\mathrm{Bo}-n^2}} = \left[\tfrac{4}{27}\mathrm{Bo}(-g)^3\right]^{1/4}, \tag{20}$$

that is for each n, such that $-g\ \mathrm{Bo}/3>n^2$, there exists $k^*(n)$. Moreover, since $k^{*2}+n^2=-g\ \mathrm{Bo}/3$, the maximum growth rate λ^* is exactly the same for all k^*'s and is independent of the mode number n! This curious behavior is illustrated in Fig. 7. However, the range of unstable wavenumbers, defined by $k^2<-(g/3)\mathrm{Bo}-n^2$, does depend upon the mode number n. Also, for illustration, the first few harmonics are shown in physical space in Fig. 8. Obviously, depending upon the value of the Bond number, one can get wavenumbers, which are multiplicative and thus there can be a possibility of three-wave resonance, with all the ensuing nontrivial nonlinear dynamics.

At the linear level, the above result implies that if only one critical wavenumber is excited, then the pattern is regular, while for higher values of Bond number or acceleration more than one critical wavenumber is excited such that the picture will likely become "frustrated," cf. Fig. 9, as was discovered recently in the experimental study of the drop splash problem by Krechetnikov and Homsy.[9] The frustration picture occurs due to randomness of the initial conditions,

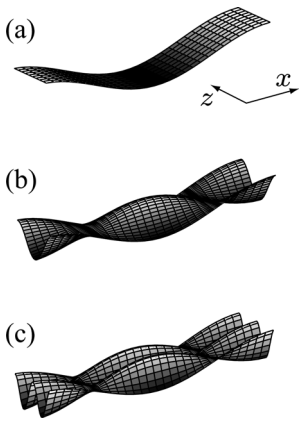

FIG. 8. Three first even modes of instability $\sim\cos n\theta\,\mathrm{Re}(e^{ikx})$: (a) $n=0$, (b) $n=1$, and (c) $n=2$.

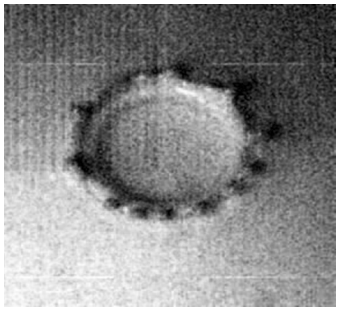

FIG. 9. Frustration phenomena (Ref. 9).

which are amplified and evolved into several superimposed patterns of different wavenumbers;[32] accordingly, these patterns are positioned with respect to each other in a random manner. As a result, for larger numbers of critical k^*'s the pattern may appear irregular, as suggested by experimental evidence.[9] These phenomena certainly necessitate further exploration, which is beyond the scope of this work: Such study will require inclusion of the effects of second curvature, unsteady acceleration, etc., in a full analysis.

Given this basic understanding of the along-the-edge instability in the flattop case, the two natural questions arise: (1) how does unsteadiness affect this instability and (2) how does the curvature of an edge change the above result? While the latter requires a separate study, which will be done in Sec. IV, the former is dealt with in Sec. III B.

B. Effects of unsteadiness

While the effect of retraction was discussed in Sec. II D and shown to be unimportant for $\mathrm{Bo}\gg 1$, another natural source of unsteadiness is the change in the liquid sheet thickness, as happens, for example, in the drop splash problem.[9] The fact that the ejecta (from which the crown is formed) travels over the time of its existence Δt in the direction of "ejection" on a greater length Δl than the change in thickness Δh it experiences,[9] indicates that its thickness evolves with a slower rate $\Delta h/\Delta t\ll\Delta l/\Delta t$.

In general, the time-evolving thickness of a liquid sheet implies that the base state is time-dependent, which calls into question the standard normal mode analysis. However, if the thickness changes on a slower time scale t_{thk} than the characteristic time of instability defined by Eq. (14), i.e., if

$$t_{\mathrm{ins}} \ll t_{\mathrm{thk}} \Leftrightarrow \mathrm{Bo}^{-1/4} \ll t_{\mathrm{thk}}/t^*, \tag{21}$$

then a quasistatic stability analysis is feasible. Namely, the only difference from the steady dispersion relation (19) is that the discrete wavenumber n is replaced by $n/h(\epsilon t)$, and so the growth rate expression becomes

$$\lambda^2 = -\sqrt{\frac{n^2}{h^2(\epsilon t)}+k^2}\left[\mathrm{Bo}^{-1}\left(\frac{n^2}{h^2(\epsilon t)}+k^2\right)+g\right], \tag{22}$$

where $\epsilon=t^*/t_{\mathrm{thk}}\ll\mathrm{Bo}^{1/4}$ indicates that the sheet thickness evolves on a slower time scale compared to the instability. The dispersion relation (22) physically implies that as the liquid sheet thickness changes in time, the pattern should change as well, even at the linear level of description, except

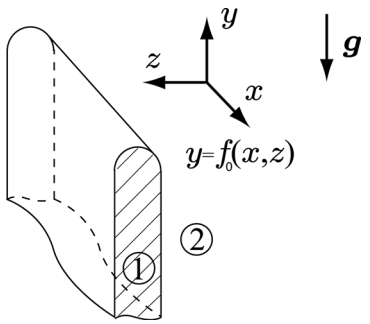

FIG. 10. Curved edges: base state with semicircular edge.

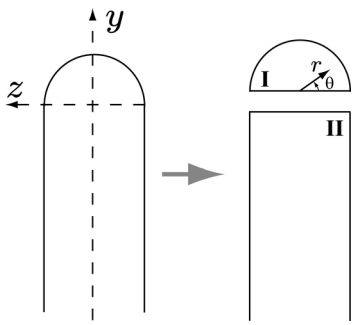

FIG. 11. Domain decomposition.

for the critical wavenumber corresponding to $n=0$ (!), because in this case (22) does not depend upon $h(\epsilon t)$.

IV. ROUNDED EDGES

A. Linear stability equations

As a reasonable approximation of a rounded edge, assume that the edge of semicircular cross-section is attached to a uniform thickness sheet, as in Fig. 10. Adopting a cylindrical coordinate system, the normal vector is

$$\boldsymbol{n} = \frac{\boldsymbol{i}_r f_r - \boldsymbol{i}_\theta f_\theta / r - \boldsymbol{i}_x f_x}{\sqrt{1 + f_\theta^2/r^2 + f_x^2}} \tag{23}$$

and the curvature is given by

$$\nabla \cdot \boldsymbol{n} = \frac{1}{r}\frac{\partial}{\partial r}(r n_r) + \frac{1}{r}\frac{\partial n_\theta}{\partial \theta} + \frac{\partial n_x}{\partial x}, \tag{24}$$

where n_r, n_θ, and n_x are the coordinate components of the normal vector in cylindrical coordinates. Equations linearized about the steady base state f_0 are rendered in the quasi-steady approximation

$$\frac{\partial \phi'}{\partial t} = -p' - g f' \sin\theta, \tag{25a}$$

$$\frac{\partial f'}{\partial t} = -\frac{\partial \phi'}{\partial r}, \tag{25b}$$

$$p' = \mathrm{Bo}^{-1}\left[\frac{f'}{f_0^2} + \frac{f'_{\theta\theta}}{f_0^2} + f'_{xx}\right], \tag{25c}$$

where ϕ' is the general solution of the Laplace equation (1a) in the region defined by the interface f_0.

Since we are interested in the along-the-edge instability, Fourier transforming in the x-coordinate, we arrive at the following system of equations:

$$\frac{\partial \hat{\phi}}{\partial t} = -\hat{p} - g\hat{f}\sin\theta, \tag{26a}$$

$$\frac{\partial \hat{f}}{\partial t} = -\frac{\partial \hat{\phi}}{\partial r}, \tag{26b}$$

$$\hat{p} = \mathrm{Bo}^{-1}\left[\frac{\hat{f}}{f_0^2} + \frac{\hat{f}_{\theta\theta}}{f_0^2} - k^2\hat{f}\right], \tag{26c}$$

where the variables with "hats" stand for the Fourier amplitudes. A special form of the Lagrange–Cauchy integral (26a) should be commented upon here: the gravity term contains dependence on $\sin\theta$ since the projection of the gravity vector on the r-component of linear momentum is $-g\sin\theta$; this will entail some nontrivial consequences in the stability analysis.

B. General solution for the velocity potential

As we learned in the previous two sections, the stability analysis requires a general solution of the Laplace equation. Obviously, in the case of the interface shown in Fig. 10, the construction of a globally valid analytical solution is a prohibitive task. However, one can utilize two important facts, namely, that the domain is a combination of two "nice" domains, as shown in Fig. 11, over which separation of variables is possible, and that we need a general solution of the Laplace equation. First, we already know a general solution for the rectangular semi-infinite strip domain (region II), which is given by Eq. (17). The task now is to construct a general solution in the semicircular bar domain (region I), which is matchable with the solution in region II. Essentially we follow the domain decomposition techniques in acoustics and other fields.[33]

The Laplace equation in region I becomes a Helmholtz equation after Fourier transformation in the x-direction,

$$\frac{1}{r}\frac{\partial}{\partial r}\left(r\frac{\partial \hat{\phi}}{\partial r}\right) + \frac{1}{r^2}\frac{\partial^2 \hat{\phi}}{\partial \theta^2} - k^2\hat{\phi} = 0. \tag{27}$$

Separating variables as

$$\hat{\phi}(r,\theta) = R(r)T(\theta) \tag{28}$$

yields two equations

$$\frac{\partial^2 T}{\partial \theta^2} + \nu^2 T = 0, \tag{29}$$

$$\rho^2\frac{\partial^2 R}{\partial \rho^2} + \rho\frac{\partial R}{\partial \rho} - (\nu^2 + \rho^2)R = 0, \tag{30}$$

where $\rho = kr$. The bounded solution of the latter equation for $\rho \to 0$ is the modified Bessel function $I_\nu(\rho)$, $\mathrm{Re}(\nu) \geq 0$. This

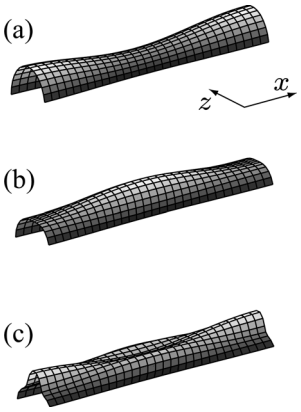

FIG. 12. Three first modes of instability $\sim\cos 2n\theta\,\mathrm{Re}(e^{ikx})$: (a) $n=0$, (b) $n=1$, and (c) $n=2$.

means that, in general, all continuous indices $\mathrm{Re}(\nu)\geq 0$ need to be summed up. However, as we will see below, the symmetry restrictions and the necessity to match the solution to the one in region II require the index ν to be natural even numbers.

Noting that the real part of solution (17) in region II is symmetric with respect to the y-axis, i.e., $\sim\cos nz$, we restrict ourselves to solutions, which are symmetric with respect to the y-axis everywhere. In particular, for $y>0$ this means that

$$\hat{\phi}(\theta)=\hat{\phi}(\pi-\theta),\quad \theta\in[0,\pi], \tag{31}$$

and thus

$$T\sim\cos 2n\theta. \tag{32}$$

This is consistent with the symmetry of the solution for $y\leq 0$, which is $\sim\cos nz$, since the latter contains only even powers of z. Now, recalling that $z=-r\cos\theta$, we can see that even powers of z for $y\leq 0$ are "matchable" with $\cos 2n\theta$ for $y\geq 0$. As a result, the general solution for the velocity potential in region I is

$$\hat{\phi}(k;r,\theta)=\sum_{n=0}^{+\infty}\phi_{kn}(t)I_{2n}(kr)\cos 2n\theta. \tag{33}$$

Since the interfacial perturbations follow the same spectral representation, one can picture the first few modes, as in Fig. 12. Since the form of solution (33) is the same as for the even modes of the free zero-gravity jet in the classical Rayleigh–Plateau analysis in Fig. 17(b) below, the stability results coincide in the absence of acceleration, i.e., $g=0$.

C. Dispersion relation and its analysis

The dispersion relation is obtained in the same fashion as done in Secs. II B and III, i.e., one substitutes the spectral representations for the velocity potential (33), interface perturbation, $\hat{f}=\Sigma f_{kn}\cos 2n\theta$, and pressure, $\hat{p}=\Sigma p_{kn}\cos 2n\theta$, into system (25) and projects onto the adjoint spectral space $\cos 2m\theta$, i.e., via multiplying by harmonics $\cos 2m\theta$ and integrating over $\theta\in[0,\pi]$, and to finally arrive at

$$I_{2n}(kf_0)\frac{\mathrm{d}\phi_{kn}}{\mathrm{d}t}=-p_{kn}-\langle,\rangle_{n,n}^{-1}g\sum_{m=0}^{\infty}f_{km}\times\int_0^{\pi}\cos 2m\theta\cos 2m\theta\sin\theta\,\mathrm{d}\theta, \tag{34a}$$

$$\frac{\mathrm{d}f_{kn}}{\mathrm{d}t}=-kI_{2n}'(kf_0)\phi_{kn}, \tag{34b}$$

$$p_{kn}=\frac{\mathrm{Bo}^{-1}}{f_0^2}[1-(2n)^2-k^2f_0^2]f_{kn}, \tag{34c}$$

where we utilized orthogonality of $\cos 2n\theta$ and $\cos 2m\theta$ on the domain $\theta\in[0,\pi]$ for $n\neq m$,

$$\langle,\rangle_{n,m}\equiv\int_0^{\pi}\cos 2n\theta\cos 2m\theta\,\mathrm{d}\theta=\begin{cases}\pi, n=m=0,\\ \pi/2, n=m\geq 1,\\ 0, n\neq m,\end{cases}$$

and where the integral

$$\int_0^{\pi}\cos 2n\theta\cos 2m\theta\sin\theta\,\mathrm{d}\theta=-\left[\frac{1}{1-4(n+m)^2}+\frac{1}{1-4(n-m)^2}\right],$$

is a general function of n,m due to nonorthogonality of the gravity vector to coordinate vectors $(\boldsymbol{i}_r,\boldsymbol{i}_\theta)$ or in other words, to the spectral directions in the domain with cylindrical symmetry.

Because of that property, the final evolution equation for f_{kn},

$$\frac{\mathrm{d}^2f_{kn}}{\mathrm{d}t^2}=-k\frac{I_{2n}'(kf_0)}{I_{2n}(kf_0)}\left\{g\left[\frac{2-16n^2}{1-16n^2}\right]\langle,\rangle_{n,n}^{-1}-\frac{\mathrm{Bo}^{-1}}{f_0^2}[1-(2n)^2-k^2f_0^2]\right\}f_{kn}-\langle,\rangle_{n,n}^{-1}k\frac{I_{2n}'(kf_0)}{I_{2n}(kf_0)}g\times\sum_{m\neq n}\left\{\frac{1}{1-4(n+m)^2}+\frac{1}{1-4(n-m)^2}\right\}f_{km}, \tag{35}$$

turns out to be coupled to all other amplitudes f_{km}, although the coupling strength between nth and mth modes decays with the distance between the modes as $\sim(n-m)^{-2}$, i.e., as the distance $|n-m|$ from the diagonal. This allows one to analyze a truncation of Eq. (35) numerically and to reach convergence with the size of the truncated system. Next, letting $f_{kn}\sim e^{\lambda_n t}\tilde{f}_{kn}$ and denoting the coefficients of f_{km} in Eq. (35) by α_{nm}, we get an infinite-dimensional system

$$\lambda_n^2\tilde{f}_{kn}=\sum_m\alpha_{nm}\tilde{f}_{km}. \tag{36}$$

The dispersion relation is formally just

$$\det(\boldsymbol{\lambda}^2\cdot\boldsymbol{I}-\boldsymbol{\alpha})=0. \tag{37}$$

Ignoring the coupling for a moment, i.e., considering just the diagonal part (35), one can notice that the corresponding dispersion relation

$$\lambda^2 = -k\frac{I'_{2n}(kf_0)}{I_{2n}(kf_0)}\left\{ g\left[\frac{2-16n^2}{1-16n^2}\right]\langle,\rangle^{-1}_{n,n} - \frac{\mathrm{Bo}^{-1}}{f_0^2}[1-(2n)^2-k^2f_0^2]\right\},$$

has a structure similar to that for Rayleigh–Plateau instability of a free jet of radius R_0,[28] given here in dimensional form ($\bar{\lambda}$ stands for the dimensional eigenvalue),

$$\bar{\lambda}^2 = \frac{\sigma}{R_0^3\rho}\frac{kR_0I'_{2n}(kR_0)}{I_{2n}(kR_0)}[1-(kR_0)^2-n^2], \tag{38}$$

but with a few crucial differences. Since $kR_0I'_{2n}(kR_0)/I_{2n}(kR_0)>0$ for all $kR_0\neq 0$, in the classical case the jet is unstable, $\bar{\lambda}^2>0$, only if $n=0$ and thus only to axisymmetric modes whose wavelength $2\pi/k$ is greater than the circumference $2\pi R_0$ of the jet. In our case though, the edge is unstable if

$$g\left[\frac{2-16n^2}{1-16n^2}\right]\langle,\rangle^{-1}_{n,n} - \frac{\mathrm{Bo}^{-1}}{f_0^2}[1-(2n)^2-k^2f_0^2]<0,$$

which holds not only for $n=0$, as in the case of free jets, but also for higher values of n, if $g<0$, depending upon the value of the Bond number.

This intuition is confirmed by analysis of the complete dispersion relation (37), which is done numerically via truncating Eq. (35) and achieving convergence with the size of the truncation. Namely, the nonzero curvature of the edge does not change the main result observed for flat edges, i.e., that in general there are a few critical wavenumbers, but the presence of curvature upsets the fact that the growth rates of those critical wavenumbers are exactly the same. This is illustrated in Fig. 13(a), which suggests that physically there may be a dominating pattern with one wavenumber and a number of superimposed secondary patterns provided all of them evolve from initial conditions of the same amplitude. For higher values of acceleration, the difference in growth rates becomes smaller, as shown in Fig. 13(b) and thus, the overall pattern may look frustrated as in Fig. 9. Finally, the limit of zero acceleration in the dispersion relation (37) clearly demonstrates that the along-the-edge instability involves both Rayleigh–Taylor and Rayleigh–Plateau mechanisms. Namely, the absence of acceleration leads to substantial weakening of the instability, as the leading growth rate corresponding to $n=0$ in Fig. 13(b) is much smaller than that in Fig. 13(a), which is due to the fact that of the two mechanisms only the Rayleigh–Plateau mechanism remains. Further decrease of the acceleration magnitude to negative values can make the edge stable! This again indicates a complicated interplay of the Rayleigh–Taylor and Rayleigh–Plateau mechanisms, which cannot be considered here just as a linear superposition of noninteracting modes, as is also evident from the nondiagonal structure of Eq. (35).

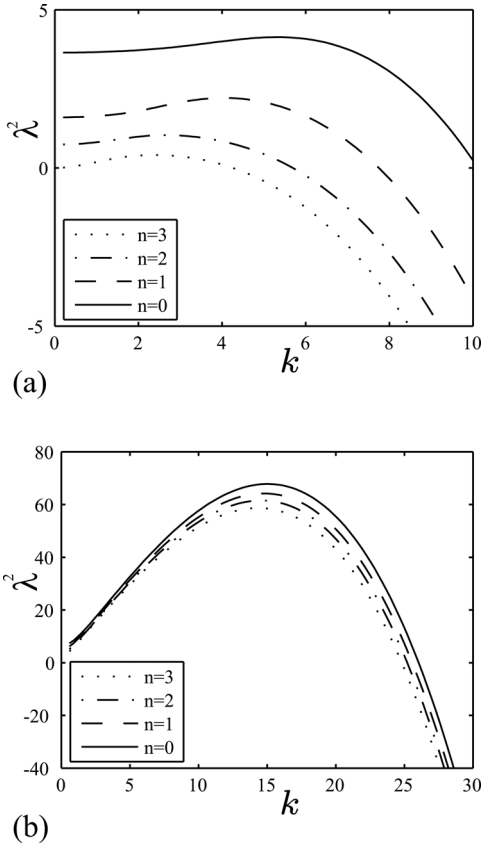

FIG. 13. Growth rates in the case of rounded edges: (a) $\mathrm{Bo}=10^2$, $g=-1$, and $f_0=1$, and (b) $\mathrm{Bo}=10^2$, $g=-10$, and $f_0=10$.

V. BLOB-EDGES

In this section, we consider the case when the edge is a well-developed blob of a radius substantially greater than the liquid sheet it attaches to, as illustrated in Fig. 14. In this situation, one just needs to construct a solution of the Laplace equation [or Helmholtz equation (27) in Fourier space] in the jet region. In fact, this harmonic solution is the same as in the study of the Rayleigh–Plateau instability[28]

$$\hat{\phi}(r,\theta) = \sum_{n=0}^{\infty}(\phi_{kn}^{(c)}\cos n\theta + \phi_{kn}^{(s)}\sin n\theta)I_n(kr), \tag{39}$$

where we have separated the even and odd components. The other two dependent variables, $\hat{f}$ and $\hat{p}$, have similar representations. Because both even and odd harmonics are present

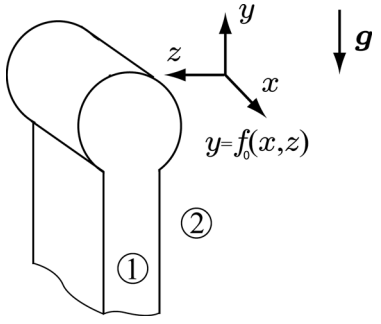

FIG. 14. Base state blob-edge.

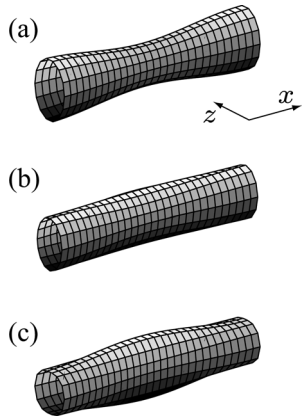

FIG. 15. The first three even modes of instability: $\sim\cos n\theta\,\mathrm{Re}(e^{ikx})$: (a) $n=0$, (b) $n=1$, and (c) $n=2$.

in this case, the leading order instability picture is more complicated compared to flat and rounded edges, as one can learn from the shape of the instability modes in Figs. 15 and 16.

Eliminating pressure and velocity potential, the resulting linear evolution system for even and odd components of the interfacial perturbations is

$$k^{-1}\frac{I_n(kf_0)}{I_n'(kf_0)}\frac{\mathrm{d}^2 f_{kn}^{(c)}}{\mathrm{d}t^2}=\left\{\frac{\mathrm{Bo}^{-1}}{f_0^2}[1-n^2-k^2f_0^2]\right\}f_{kn}^{(c)}+\frac{g}{\langle,\rangle_{n,n}^{(c)}}\sum_{m=0}^{\infty}a_{nm}^{(s)}f_{km}^{(s)},\tag{40a}$$

$$k^{-1}\frac{I_n(kf_0)}{I_n'(kf_0)}\frac{\mathrm{d}^2 f_{kn}^{(s)}}{\mathrm{d}t^2}=\left\{\frac{\mathrm{Bo}^{-1}}{f_0^2}[1-n^2-k^2f_0^2]\right\}f_{kn}^{(s)}+\frac{g}{\langle,\rangle_{n,n}^{(s)}}\sum_{m=0}^{\infty}a_{nm}^{(c)}f_{km}^{(c)},\tag{40b}$$

where

$$\langle,\rangle_{n,m}^{(c)}\equiv\int_0^{2\pi}\cos n\theta\cos m\theta\,\mathrm{d}\theta=\begin{cases}2\pi, n=m=0,\\ \pi, n=m\geq 1,\\ 0, n\neq m,\end{cases}\tag{41}$$

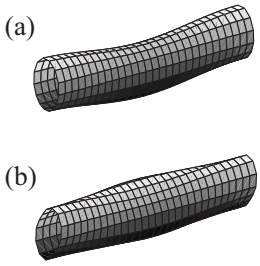

FIG. 16. The first three odd modes of instability: $\sim\sin n\theta\,\mathrm{Re}(e^{ikx})$: (a) $n=1$ and (b) $n=2$.

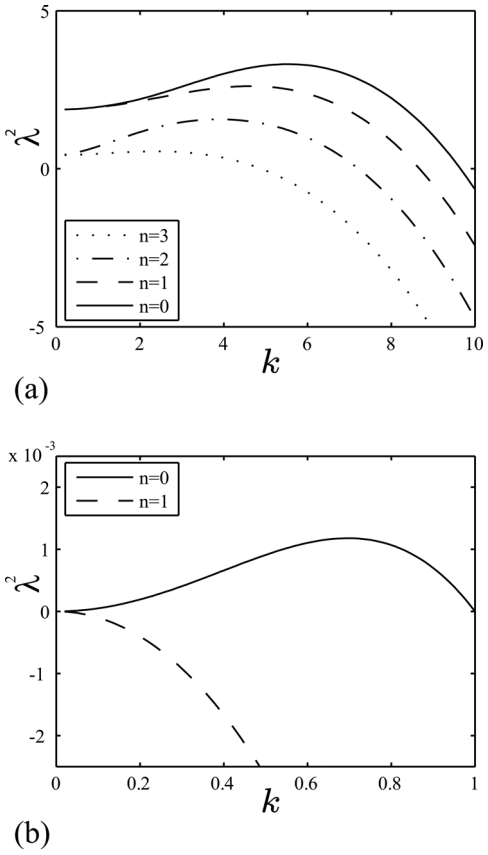

FIG. 17. Growth rates in the case of blob-edges: (a) $\mathrm{Bo}=10^2$, $g=1$, and $f_0=1$, and (b) $\mathrm{Bo}=10^2$, $g=0$, and $f_0=1$.

$$\langle,\rangle_{n,m}^{(s)}\equiv\int_0^{2\pi}\sin n\theta\sin m\theta\,\mathrm{d}\theta=\begin{cases}0, n=m=0,\\ \pi, n=m\geq 1,\\ 0, n\neq m,\end{cases}$$

and the coupling matrices are

$$\boldsymbol{a}^{(s)}=\begin{pmatrix}\pi & 0 & 0 & \\ 0 & \frac{\pi}{2} & 0 & \\ -\frac{\pi}{2} & 0 & \frac{\pi}{2} & \ddots \\ 0 & -\frac{\pi}{2} & 0 & \ddots \\ & \ddots & \ddots & \ddots\end{pmatrix},\quad \boldsymbol{a}^{(c)}=[\boldsymbol{a}^{(s)}]^T.\tag{42}$$

Next, letting $f_{kn}\sim e^{\lambda_n t}\tilde{f}_{kn}$ we get a dispersion relation analogous to Eq. (37), but with very sparse matrices due to the form of Eq. (42). Its analysis demonstrates that, as opposed to the classical zero-gravity free jet analysis[28] shown for reference in Fig. 17(b), the acceleration allows the existence of several instability modes, e.g., for $n=0$ and $n=1$ in Fig. 17(a). Again, in analogy to the conclusions drawn from the study of flattop edges, there can be several critical wavenumbers excited.

Similar to the case of rounded edges considered earlier, the limit of zero acceleration in the corresponding dispersion relation again demonstrates that the instability has two inter-

acting components—Rayleigh–Taylor and Rayleigh–Plateau mechanisms. This is also suggested by nondiagonal structure of the dispersion relation and since in the absence of acceleration the instability is weakened. The case of negative accelerations is identical to the one for positive values of acceleration because of the symmetry of the blob in the y-direction, i.e., the instability picture is invariant with respect to the transformation $g \to -g$. It should be noted that we treated blob-edges as free jets, which is justified by the small influence of the fluid-fluid contact between the blob and the attached thin liquid sheet due to negligible inertia of the latter. This is opposed to the case of a liquid jet contacting a fixed (and thus of infinite inertia) solid wire studied by Davis,[34] where the effect of the contact line seems to change the range of unstable wavenumbers at the leading order. However, the cases of a semicircular jet on a solid surface and a rounded liquid sheet edge, studied in Sec. IV, are analogous in the sense that the presence of a contact line and a finite thickness sheet has the leading order effect on the range of unstable wavenumbers.

VI. CONCLUSIONS

The systematic study of longitudinal (along-the-edge) instabilities of accelerated flat, rounded, and blob-edges in this work has revealed the underlying physical mechanisms, and, in particular, the fact that the growing disturbances owe their existence to two mechanisms—Rayleigh–Taylor and Rayleigh–Plateau instabilities—which cannot be considered simply as a linear superposition of noninteracting modes. Thus, the resulting stability picture cannot be inferred from the classical studies of Rayleigh–Taylor instability for flat interfaces and the Rayleigh–Plateau instability of a round jet. Therefore, the interplay of these two instabilities leads to a number of nontrivial results.

In particular, it is discovered in the case of flat edges that several critical wavenumbers may coexist with the same growth rates. Physically, this leads to frustration phenomena, when several along-the-edge wavelengths compete with each other; since the pattern is dictated by the initial conditions, the resulting picture may appear irregular. Curvature of the edge, i.e., in the case of rounded and blob-edges, distorts somewhat this equal amplification of different critical wavenumbers, but still allows for several critical wavenumbers to coexist.

While this study gives quantitative information about instability in the quasisteady case only, it also provides an important insight for the cases when Bo is not large by suggesting that the perturbation penetrates into the liquid sheet on the distance of the order of the sheet thickness and thus invalidates the application of the classical Rayleigh–Taylor analysis for flat infinite interfaces.

This work was also limited to planar sheets subject to inviscid irrotational disturbances, so possible extensions would include effects of viscosity and a second curvature. Such extensions would make the analysis relevant, for example, to the drop splash problem, where the question of predicting the number of spikes along the rim,[25] remains open in view of the complexity of the splash phenomena (i.e., highly unsteady acceleration of the rim and nontrivial time-dependence of the liquid sheet (ejecta) thickness, cf. Ref. 9).

In conclusion, it is worth mentioning that liquid sheet edges also occur when a jet impacts a small disk so that a radially expanding film is formed, which disintegrates along its periphery with the drop formation process at its rim.[6,35] The mechanism of this disintegration is different, however, from the instability considered here, which is due to acceleration of the entire sheet combined with the Rayleigh–Plateau mechanism. Namely, the disintegration of a radially expanding sheet is either due to local acceleration near the edge induced by flapping (when the friction with the surrounding air is strong enough to trigger Kelvin–Helmholtz instability)[6] or solely due to the Rayleigh–Plateau mechanism for smooth liquid sheets.[35]

ACKNOWLEDGMENTS

The author gratefully acknowledges insightful discussions with Professor Bud Homsy and constructive criticism of the referees.

[1] D. R. Brown, "A study of the behaviour of a thin sheet of a moving liquid," J. Fluid Mech. **10**, 297 (1961).
[2] K. Miyamoto and Y. Katagiri, "Curtain coating," in *Liquid Film Coating*, edited by S. Kistler and P. Schweizer (Chapman and Hall, Cambridge, 1997), pp. 463–494.
[3] A. H. Lefebvre, *Atomization and Sprays* (Hemisphere, New York, 1989).
[4] J. S. Roche, N. Le Grand, P. Brunet, L. Lebon, and L. Limat, "Perturbations on a liquid curtain near break-up: Wakes and free edges," Phys. Fluids **18**, 082101 (2006).
[5] C. Clanet, "Waterbells and liquid sheets," Annu. Rev. Fluid Mech. **39**, 469 (2007).
[6] E. Villermaux and C. Clanet, "Life of a flapping liquid sheet," J. Fluid Mech. **462**, 341 (2002).
[7] A. Rozhkov, B. Prunet-Foch, and M. Vignes-Adler, "Impact of water drops on small targets," Phys. Fluids **14**, 3485 (2002).
[8] R. D. Deegan, P. Brunet, and J. Eggers, "Complexities of splashing," Nonlinearity **21**, C1 (2008).
[9] R. Krechetnikov and G. M. Homsy, "Crown-forming instability phenomena in the drop splash problem," J. Colloid Interface Sci. **331**, 555 (2009).
[10] G. I. Taylor, "The instability of liquid surfaces when accelerated in a direction perpendicular to their planes. I. Waves on fluid sheets," Proc. R. Soc. London, Ser. A **201**, 192 (1950).
[11] F. E. C. Culick, "Comments on a ruptured soap film," J. Appl. Phys. **31**, 1128 (1960).
[12] J. B. Keller, "Breaking of liquid films and threads," Phys. Fluids **26**, 3451 (1983).
[13] M. P. Brenner and D. Gueyffier, "On the bursting of viscous films," Phys. Fluids **11**, 737 (1999).
[14] G. Debrégeas, P.-G. de Gennes, and F. Brochard-Wyart, "The life and death of 'bare' viscous bubbles," Science **279**, 1704 (1998).
[15] G. Debrégeas, P. Martin, and F. Brochard-Wyart, "Viscous bursting of suspended films," Phys. Rev. Lett. **75**, 3886 (1995).
[16] M. Song and G. Tryggvason, "The formation of thick borders on an initially stationary fluid sheet," Phys. Fluids **11**, 2487 (1999).
[17] G. Sünderhauf, H. Raszillier, and F. Durst, "The retraction of the edge of a planar liquid sheet," Phys. Fluids **14**, 198 (2002).
[18] I. V. Roisman, K. Horvat, and C. Tropea, "Spray impact: Rim transverse instability initiating fingering and splash, and description of a secondary spray," Phys. Fluids **18**, 102104 (2006).
[19] J. M. Fullana and S. Zaleski, "Stability of a growing end rim in a liquid sheet of uniform thickness," Phys. Fluids **11**, 952 (1999).
[20] S. P. Lin, *Breakup of Liquid Sheets and Jets* (Cambridge University Press, Cambridge, 2003).
[21] W. A. Sirignano and C. Mehring, "Review of theory of distortion and disintegration of liquid streams," Prog. Energy Combust. Sci. **26**, 609 (2000).

[22]R. Krechetnikov, "Rayleigh–Taylor and Richtmyer–Meshkov instabilities of flat and curved interfaces," J. Fluid Mech. **625**, 387 (2009).
[23]R. F. Allen, "The role of surface tension in splashing," J. Colloid Interface Sci. **51**, 350 (1975).
[24]A. M. Worthington, *A Study of Splashes* (Longmans, London, 1908).
[25]H. E. Edgerton and J. R. Killian, *Flash! Seeing the Unseen by Ultra High-Speed Photography* (Charles T. Branford, Boston, 1954).
[26]H. E. Edgerton, *Stopping Time: The Photographs of Harold Edgerton* (Abrams, New York, 1977).
[27]D. Langbein, "The shape and stability of liquid menisci at solid edges," J. Fluid Mech. **213**, 251 (1990).
[28]P. G. Drazin and W. H. Reid, *Hydrodynamic Stability* (Cambridge University Press, Cambridge, 2004).
[29]L. G. Loitsyanskii, *Mechanics of Liquids and Gases* (Pergamon, New York, 1966).
[30]L. E. Johns and R. Narayanan, *Interfacial Instability* (Springer-Verlag, New York, 2002).
[31]However, one may argue that in some situations viscous flow may be well approximated by potential motion (Ref. 36) and thus, the present analysis for an ideal fluid may be relevant to the viscous motion too; also one can imagine a situation when viscosity imposes a flat edge, while at a long-wave scale an inertia-dominated behavior takes place.
[32]Observation of this picture should be possible for moderate number of spikes along the rim. If there are too many well-developed spikes, the short distance between them may lead to their merging due to surface tension effects.
[33]A. Quarteroni and A. Valli, *Domain Decomposition Methods for Partial Differential Equations* (Oxford University Press, New York, 1999).
[34]S. H. Davis, "Moving contact lines and rivulet instabilities. Part 1. The static rivulet," J. Fluid Mech. **98**, 225 (1980).
[35]C. Clanet and E. Villermaux, "Life of a smooth liquid sheet," J. Fluid Mech. **462**, 307 (2002).
[36]D. Joseph, T. Funada, and J. Wang, *Potential Flows of Viscous and Viscoelastic Liquids* (Cambridge University Press, Cambridge, 2007).